Behavior of Cumulus Activity and the Structures of Circulations in an "Aqua Planet" Model

Part II: Eastward-Moving Planetary Scale Structure and the Intertropical Convergence Zone

By Atusi Numaguti and Yoshi-Yuki Hayashi

Department of Earth and Planetary Physics, University of Tokyo, Tokyo 113 Japan
(Manuscript received 12 December 1990, in revised form 31 July 1991)

Abstract

The results of 'aqua planet' GCM experiments are analyzed, concentrating on the planetary scale structure and the structure of precipitating areas around the ITCZ region.

The 30 day oscillations, that is, eastward-moving structures on the planetary scale, appear in a similar way regardless of the cumulus parameterization utilized. These structures are considered to be maintained by the dependence of evaporation on wind speed, *i.e.*, the evaporation–wind feedback mechanism. For the maintenance of the disturbances on the synoptic scale, this mechanism is considered to be less effective and other mechanisms such as wave-CISK are more important. It is suggested that the coexistence of two different maintenance mechanism of disturbances is relevant to the existence of hierarchical structure of cumulus activity in the model.

At the double ITCZ latitudes in the experiments with Kuo's cumulus parameterization, there are areas of high cumulus activity on the grid scale, which are moving eastward continuously. In the experiment with moist convective adjustment, on the other hand, westward-moving areas of high cumulus activity associated with vorticity, which correspond well to the easterly wave disturbances in the real tropics, are observed. It is revealed that a process which can be called 'evaporation–wind feedback for the zonal mean field' exists and contributes to the separation of the ITCZ into double bands in the experiments with Kuo's parameterization.

1. Introduction

Cumulus activity in the tropics is one of the most important elements in the general circulation of the atmosphere. Its distribution is not uniform or random. It is shown by recent studies (*e.g.*, Nakazawa, 1988) that the distribution of cumulus clouds has a hierarchical structure and each structure is closely related to the circulation field. From the results of 'aqua planet' GCM experiments, Hayashi and Sumi (1986, we call HS86 hereafter) pointed out that a hierarchical structure of cumulus activity forms spontaneously even if the boundary condition is uniform. In their results, the regions of the highest cumulus activity were located off the equator to appear as double ITCZs (intertropical convergence zones). In the narrow equatorial belt between the two ITCZs, areas of high cumulus activity of synoptic scale, with the horizontal dimension of about 3000 km, emerged and moved eastward continuously, which were named 'super clusters'. Moreover, an eastward-moving planetary scale structure of wavenumber one (30 day oscillation) also appeared as a modulation of the super clusters.

From the OLR (outgoing longwave radiation) data of the real tropics, Nakazawa (1988) detected eastward movement of cloud areas on synoptic scale which may be interpreted to correspond to HS86's super clusters. He further showed that there is a smaller scale structure within a super cluster, which is composed of several cloud clusters. The eastward-moving structure of wavenumber one in the real tropics is widely recognized as the 30–60 day oscillation or the Madden-Julian oscillation (Madden and Julian, 1972), and has been intensively investigated in a number of authors in recent observational works (*e.g.*, Knutson and Weickmann 1987, Rui and Wang, 1990). It is also a well known fact that the ITCZ prefers to appear at latitudes off the equator,

and sometimes double ITCZs form, although the radiative forcing is maximum at the equator (Hubert *et al.*, 1969). The ITCZs are observed as longitudinally oriented zones in the time mean field. At each instant, however, cumulus activity in the zones is associated with various disturbances on synoptic or even smaller scales. The well-known example is a westward-propagating disturbance which is called an 'easterly wave disturbance' (Reed and Recker, 1971).

Many attempts have been made to for explain these characteristics of the distribution of cumulus activity. However, the described images differ greatly from one model to another. Moreover, there are few works that account for this hierarchical structure *as a whole*.

The results of HS86 are suggestive in further understanding these problems. In part I of this paper (Numaguti and Hayashi, 1991), we analyzed the results of their original experiments and some additional GCM experiments with different parameters. The time and zonal mean distribution and the time-longitude sections of precipitation are described. Moreover, the structures of circulation associated with the eastward-moving precipitating areas, *i.e.*, super clusters, are examined. The results are summarized as follows:

- The 'super cluster' shown by HS86 is confirmed to exist in the model as an eastward-moving precipitating area at the equator. The horizontal scale ($\sim$1000 km) of the area is *grid scale*, which is marginally resolvable scale in the model. The '30 day oscillation' is observed as a modulation of the amount of precipitation on the planetary scale (Fig. 1a).
- The eastward-moving precipitating areas of the grid scale[1] are considered to be maintained by the wave-CISK mechanism connected with Kelvin waves.
- The dependence of the activity of the grid scale precipitating areas on SST (sea surface temperature) is opposite to that of the amplitude of the planetary scale modulation structure. When the SST is higher, the activity of the grid scale precipitating areas is higher, while the planetary scale modulation is less significant.
- There is no difference in speed between the grid scale precipitating areas at the equator and that of the planetary scale modulation structure.

[1]In order to avoid confusion between the model result and the real phenomena, we use the word 'grid scale precipitating area' rather than 'super cluster' when we describe the results of the model in the rest of this paper. Similarly, we use the word 'planetary scale (modulation) structure' instead of '30 day oscillation' or 'Madden-Julian oscillation'.

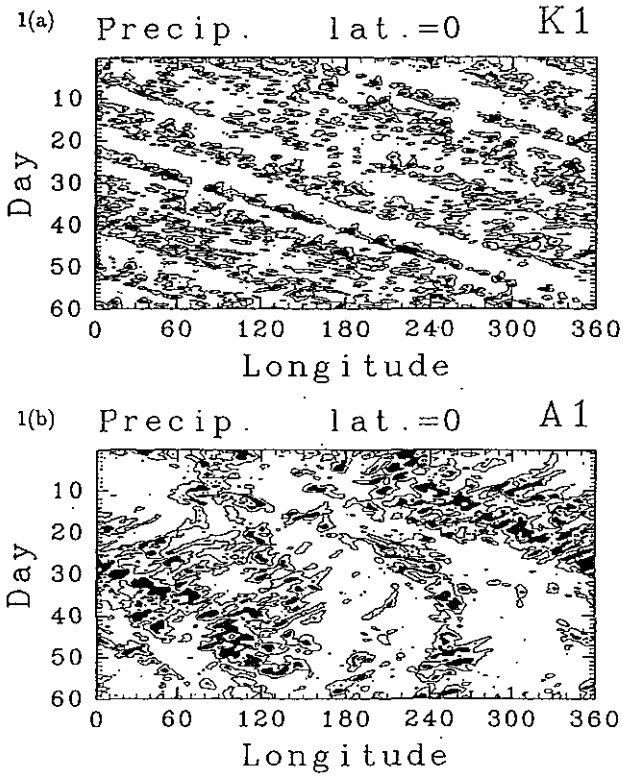

Fig. 1. Longitude–time distributions of precipitation at the equator. Contours indicate 2 mm/day and areas of over 10 mm/day are shaded. (a) Standard experiment K1, (b) experiment with moist convective adjustment A1.

- In the results of the experiment using moist convective adjustment instead of Kuo's parameterization, grid scale precipitating areas still appear but do not move continuously (Fig. 1b). On the other hand, a modulation structure of planetary scale is exhibited similarly to the case of Kuo's parameterization.
- The double ITCZ structure, which appears distinctly in the experiments with Kuo's parameterization, is rather unclear in the experiment with the moist convective adjustment.

In Part II, we will examine the results of the same experiments described in Part I, paying attention to the structure of the planetary scale modulation, which may correspond to the Madden-Julian oscillation, and the behavior of precipitation around the latitudes of double ITCZs. The main concerns in this paper are the mechanisms of the maintenance of those structures. In recent years, several mechanisms of maintenance of disturbances coupled with cumulus activity have been examined. They can be classified into three categories; frictional CISK, wave-CISK and evaporation-wind feedback (refer to Part I for the detail of the definition of these). Frictional CISK is a mechanism which maintains

a disturbance through the intensification of cumulus activity caused by frictionally controled convergence in the planetary boundary layer (Charney and Eliassen, 1964). This mechanism is usually connected with vortex-like disturbances. However, Wang (1988) showed that this mechanism can also operate in wave-like disturbances. Wave-CISK is a mechanism which maintains a disturbance through the intensification of cumulus activity enhanced by the upward motion associated with the wave itself (Hayashi, 1970; Lau and Peng, 1987). Evaporation-wind feedback (Emanuel, 1987; Neelin *et al.*, 1987) is a mechanism for the maintenance of a disturbance which operates through the dependence of evaporation on surface wind speed $|v|$ which is represented as follows:

$$E = \rho C_D |v| (q^* - q_a), \tag{1}$$

where ρ is the air density, C_D the bulk coefficient, q^* the saturation specific humidity at the surface, and q_a is the specific humidity of the air near the surface. If there is a tendency that the large evaporation enhances the heating efficiently, the disturbance can be maintained under the condition that the surface wind is strong and consequently the evaporation is large in the warm region of the disturbance. So far, there is no consensus on which mechanism is effective for the maintenance of each characteristic structure of cumulus activity.

Concerning the Madden-Julian oscillation, there are a number of studies in recent years. From observational studies, it is suggested that the propagation of the equatorial Kelvin waves is essential, which have a maximum amplitude at the equator and propagate eastward. HS86 stated that the period of 30 to 60 days is basically determined by the time required for a wave to turn around the equatorial circle, and that the cumulus activity is crucial for the maintenance of the wave. Many recent studies have presented similar ideas, although there are some studies which claim that other processes such as the fluctuation of the monsoon activity in the atmosphere–ocean–land system is an important factor for the periodicity (Webster, 1983).

It is possible to maintain Kelvin waves by any one of the processes listed previously; frictional CISK, wave-CISK and evaporation–wind feedback (Chang and Lim, 1988; Wang and Chen, 1989; Emanuel, 1987). It has not been clearly understood what mechanism is actually effective for the maintenance of Kelvin waves, although there have been a number of GCM experiments. Based on the analyses of GCM results, Lau *et al.* (1988) stated that the eastward-moving planetary scale structure is basically explained as Kelvin waves maintained by the wave-CISK process. They also showed that other processes such as frictional CISK and evaporation–wind feedback are not negligible for maintenance. Neelin *et al.* (1987) performed comparative experiments with and without the dependence of evaporation on wind speed to see if the evaporation–wind feedback process is crucial for maintenance. They found that the evaporation–wind feedback is effective for the amplification, but is not indispensable. Tokioka *et al.* (1988) also attempted to explain the propagation and maintenance of the disturbance using the concept of wave-CISK.

A deficiency of the explanation of Madden-Julian oscillation in terms of wave-CISK mechanism is incapability of correctly predicting the zonal scale selection in the linear theory. The growth rate of linear mode solution is the largest at the smallest zonal wave length. This problem of scale selection cannot be settled by introduction of frictional CISK or evaporation-wind feedback. As a matter of fact, in the linear theory of evaporation-wind feedback, the growth rate of the smallest scale is maximum (Emanuel, 1987). In the linear theory of frictional CISK, the growth rate is slightly larger for larger scales when a certain value of parameter is adopted (Wang and Chen, 1989). However, the dependence of growth rate on horizontal scale is so weak that it does not seem to explain the dominance of wavenumber one. A modification of wave-CISK addressing this failure is proposed by Lau and Peng (1987). When the nonlinear positive-only wave-CISK model which prevents the negative heating in the area of downward motion is adopted, the area of upward motion (*i.e.* heating region) is concentrated into a 2000 km scale area and the area of downward motion spreads over the remaining equatorial belt. There appears a predominance of planetary scale east-west circulation. Itoh (1989) used a similar model as Lau and Peng's including the moisture budget, and found that the selection of planetary scales is enhanced when the heating by cumulus is restricted to a region where the relative humidity is higher than a certain critical value. From these studies, the zonal scale selection appears to be explained within the wave-CISK framework. However, the results of these simple models do not show the hierarchical structure composed of super clusters and the Madden-Julian oscillation. The explanation is not consistent with the results of HS86.

HS86 stated that the following feedback mechanism might maintain the planetary scale structure. If a non-uniformity in the distribution of the super clusters exists, a Walker circulation on a planetary scale is excited. In the downward region of the circulation, occurrence of the super clusters is suppressed. This process will amplify the existing non-uniformity. However, they did not give any evidences supporting this hypothesis; their statement remains a mere speculation.

Regarding the origin of ITCZ, some studies have been done for explaining the fact that usually the

Table 1. The setup of the main experiments

Exp.	SST	cumulus parameterization
K1	standard(HS86)	Kuo (1974)
K2	+2K	Kuo (1974)
K3	−2K	Kuo (1974)
A1	standard	moist convective adjustment

ITCZ is not located at the equator. Charney (1969) considered that the frictional CISK process with vorticity is important in the formation of the ITCZ. He supposed that the formation of an ITCZ at the equator is difficult because the Coriolis effect is absent there and consequently the frictional CISK mechanism does not operate. Pike (1971) performed some experiments with a simple ocean-atmosphere coupled model and claimed that the low sea surface temperature at the equator, generated by oceanic upwelling, is a necessary condition for the shift of the ITCZ from the equator. The results of realistic GCM simulations by Manabe *et al.* (1974) show that the latitude of the ITCZ follows the seasonal migration of the latitude of the peak sea surface temperature. This result agrees with Pike (1971)'s view of the ITCZ. In contrast to these results, the result of HS86 shows that the atmosphere itself prefers to have non-equatorial ITCZs, and seems to support Charney's (1969) idea. However, it has not been examined yet whether the generation of double ITCZs in the HS86's model is due to the frictional CISK process or not.

Stimulated by these circumstances and the results of Part I, we will examine further the results of experiments described in Part I. Firstly, the circulation structures of the planetary scale modulation, *i.e.*, the 30 day oscillation, are examined and the mechanism of the maintenance is discussed. Secondly, in order to discuss the structure of ITCZs and their origin, the behavior of precipitation at around the latitudes of the double ITCZs and associated disturbance structure are analyzed. A brief description of the model and experiments is given in Section 2. The results of the analyses are presented in Sections 3 and 4, concerning the results of the experiments with Kuo's cumulus parameterization and with the moist convective adjustment scheme, respectively. Discussion on the results is given in Section 5.

2. The model and experiments

2.1 The model

The GCM experiments examined here are the same set of experiments described in Part I. Thus the descriptions of the model and experimental setup are mentioned only briefly. Readers are referred to Part I for more details.

The model used in this study is a global spectral model originally developed by the Japan Meteorological Agency (Kanamitsu *et al.*, 1983), which is virtually the same model used by HS86. The horizontal resolution is triangular 42 and the physical processes are calculated at grid points located at approximately every 2.8 degrees. The model has 12 levels in the vertical direction. In the first three main experiments (see Table 1), the parameterization of Kuo (1974), which is the same as HS86 used, is adopted as the cumulus parameterization. In the other main experiment, the moist convective adjustment scheme (Manabe *et al.*, 1965) is adopted.

2.2 Setup of experiments

Four series of time integrations were performed as the main experiments. The basic parameters of the experiments are the same as HS86. The whole surface is covered with an 'ocean', in which the value of the sea surface temperature(SST) is prescribed as a function of latitude only and completely wetted. The surface albedo is taken to be longitudinally uniform. The location of the sun is fixed at the the equinox position and no seasonal variation is allowed, though the diurnal variation is included.

The setup of the experiments is summarized in Table 1. The SST distribution for the standard experiment (K1) is the same as HS86's. That is hemispherically symmetric and zonally uniform with a peak at the equator. The SST is increased by 2K everywhere in experiment K2, whereas the SST is decreased by 2K everywhere in experiment K3. Experiment A1 is the same as experiment K1 except for the different cumulus parameterization. In each experiment, the model is integrated for 120 days, and the data of the last 60 days are used for analyses.

3. Experiments with Kuo's parameterization

3.1 Eastward-propagating planetary scale structure around the equator

The structure of the eastward-propagating planetary scale modulation is basically the same as that described in HS86. As mentioned in Part I, the planetary scale modulation is more evident in the low SST experiment K3, than in experiments K1 and K2. Thus the structure of the circulation in experiment K3 is described here as the representative one. The characteristics are qualitatively the same in other experiments as long as the modulation appears. The circulation fields of the planetary scale modulation structure are shown in Fig. 2 which are

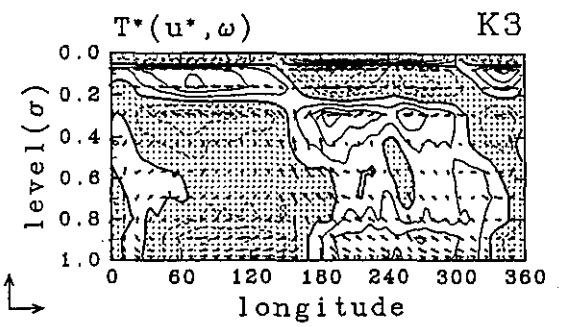

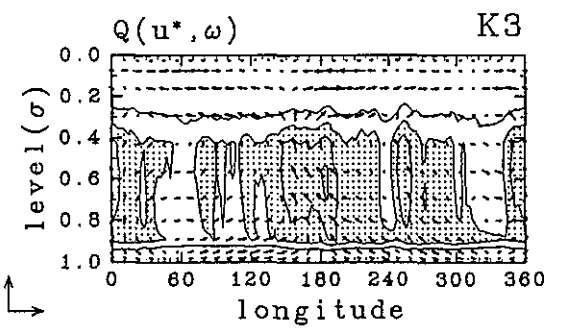

Fig. 2. Composite structure in experiment K3 with reference to a point moving at a constant speed (10 m/s). (a) Longitude–height section of temperature (contour) and wind vectors at the equator. Zonal means are subtracted for temperature and zonal wind. The contour interval is 0.1K and negative areas are shaded. (b) Longitude–height section of cumulus heating (contour) and wind vectors at the equator. Zonal mean is subtracted for zonal wind. The contour interval is 0.5K/day and areas of over 1K/day are shaded. In each figure, the unit vectors shown at the left side bottom represent 5 m/s and 2.5 mb/hr respectively.

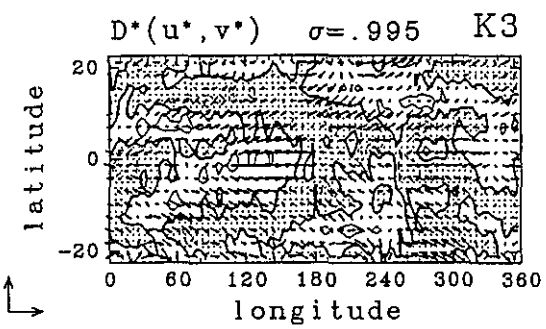

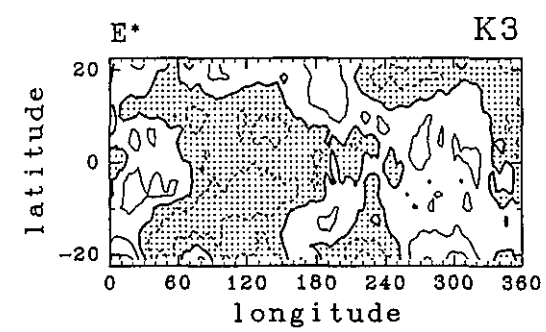

Fig. 3. Horizontal distributions of divergence and evaporation in experiment K3 in the composite with reference to a point moving at a constant speed (10 m/s). (a) Divergence (contour) and wind vectors at $\sigma = 0.995$ (about 995 mb). Zonal means are subtracted for all quantities. The contour interval is $1 \times 10^{-6} s^{-1}$ and negative (convergence) areas are shaded. The unit vectors shown at the left side bottom represent 2.5 m/s for both directions. (b) Evaporation from surface. Zonal mean is subtracted. The contour interval is 5 W/m^2 (corresponding to about 0.2 mm/day precipitation) and negative areas are shaded.

produced using a composite technique. The composite is made with reference to a key point which is moving at a constant speed (10 m/s) corresponding to the propagation speed of the planetary scale structure. The fields of zonal velocity and temperature (see Fig. 2a) show a wavenumber-one structure which is slanted westward with increasing altitude. Its vertical structure in the troposphere is the so called 'first baroclinic mode' whose horizontal velocities in the upper troposphere and in the lower troposphere are in opposite direction. There seems to be a certain structure over the tropopause, but it will not be of concern here, because the resolution is not sufficient (only two levels in the stratosphere) and strongly influenced by a poor treatment of the upper boundary. Figure 2b is the composite distribution of heating by cumulus, which shows an indication of the large scale modulation of the heating.

In Fig. 3a, the convergence and the wind field in the planetary boundary layer ($\sigma = 0.995$) of experiment K3 are plotted. A planetary scale structure of wavenumber one or two centered at the equator clearly appears. The meridional diverging wind away from the equator is significant in the region of positive divergence around 120 degrees longitude in the figure. A clear planetary scale feature also exists in the composite evaporation field (Fig. 3b). The amplitude of the longitudinal contrast of evaporation is rather large at off-equatorial latitudes. Since the zonal mean value of evaporation is 50~100 W/m^2 as shown in Fig. 4b, the longitudinal difference of evaporation is 10 to 20 % of the mean value. This amplitude is similar to that obtained by Lau *et al.* (1988). Figure 5 represents the composite longitudinal distributions of the absolute value of surface wind speed, evaporation, and precipitation averaged between 10 degrees north and 10 degrees south. Because of the presence of a mean easterly wind (Fig. 4a), the absolute value of wind speed and

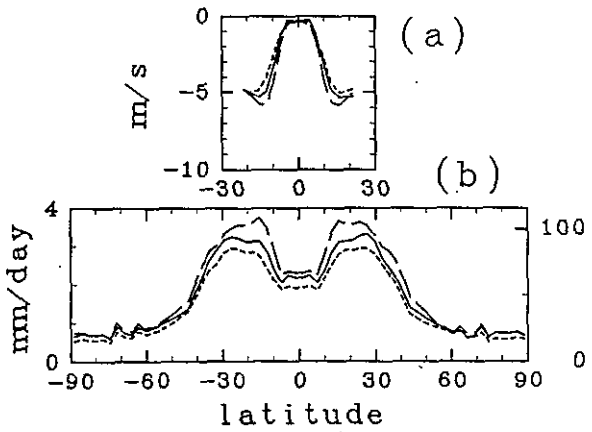

Fig. 4. Zonal and time mean distributions of surface zonal wind $[u]$ and evaporation $[E]$ fields. Solid line; standard experiment K1. Broken line; high SST experiment K2. Dotted line; low SST experiment K3. (a) Zonal wind $[u]$. at $\sigma=0.995$ (about 995 mb). Unit is m/s. (b) Evaporation $[E]$. Unit is mm/day (left) and W/m^2 (right).

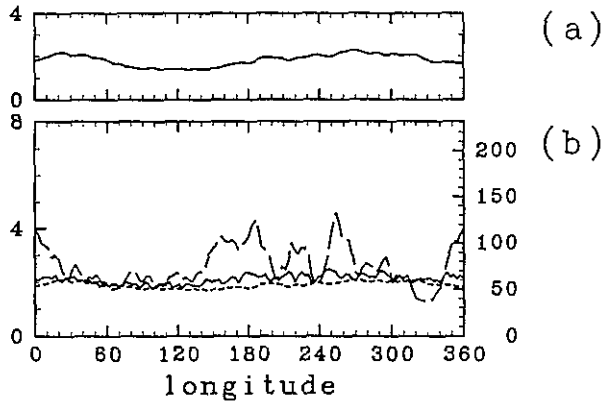

Fig. 5. Longitudinal distributions of variables related to the heating in experiment K3 averaged around the equator (+10°∼−10°) in the composite, with reference to a point moving at a constant speed (10 m/s). (a) Absolute value of wind speed near the surface ($\sigma=0.995$, about 995 mb). Unit is m/s. (b) Dotted line; evaporation. Broken line; precipitation (vertically integrated heating). Solid line; vertically integrated heating from which the adiabatic cooling is subtracted. Unit is mm/day (left) and W/m^2 (right).

consequently the evaporation are large to the east of the low level longitudinal convergence center (about 180 degrees longitude). It is the region where the temperature is relatively high (Fig. 2a). The precipitation is comparatively large in the warm region to the east of the low level longitudinal convergence center than in the cold region to the west, and hence total energy conversion to the planetary scale disturbance is expected.

A large portion of the heating by cumulus is canceled by adiabatic cooling by upward motion and not connected to the tendency of the temperature. The vertically integrated effective warming rate by cumulus and associated circulation, which is defined as the difference between the heating rate by cumulus and the adiabatic cooling rate, is also plotted in Fig. 5. It can be seen that the correlation between this effective warming and temperature (Fig. 2a) is positive. This positive correlation indicates that the net increase of the disturbance available potential energy, where the conversion to the kinetic energy with upward motion is subtracted, is positive. The net warming rate, which is the summation of this effective warming rate by cumulus and associated circulation, the heating rate by radiation and the heating rate by PBL processes, is corresponding to the local tendency of temperature and must be consistent with the eastward propagation of the temperature distribution so long as the effect of nonlinear advection is neglected. More quantitative analysis of temperature and energy budgets of the disturbance is difficult because the amplitude of the temperature signal (∼0.2K) is quite small and the time scale (∼ 50 day) is rather long, and hence, the corresponding change of vertically integrated internal energy is estimated to be less than 1 W/m^2. The longer and denser data of the model results than presently available[2] are required.

3.2 Longitude-time distribution of precipitation at 10 degrees latitude

In order to see time-dependent behavior of the precipitation at the ITCZs, the longitude–time distribution of precipitation at 10 degrees latitude in the standard experiment K1 is shown as Fig. 6a. The predominance of eastward-moving precipitating areas is readily seen. Their spatial scale is similar to the scale of the precipitating areas at the equator, that is about 1000 km (refer to Part I). The movement of the precipitating areas at this latitude is more steady than that at the equator, and the number of areas existing at one time is larger. The speed of movement is higher than that at the equator: It goes around the latitudinal circle in about 22 days. The planetary scale structure modulation is not easily seen. But by comparing this with the corresponding time-longitude section at the equator (Fig. 1a), we can trace the connection with the corresponding pattern at the equator. Planetary scale structures in Fig. 6a and Fig. 1a may be different aspects of the same structure.

In the high SST experiment K2 (Fig. 6b), the

[2]Our historical data of the experiments are sampled every 6 hours.

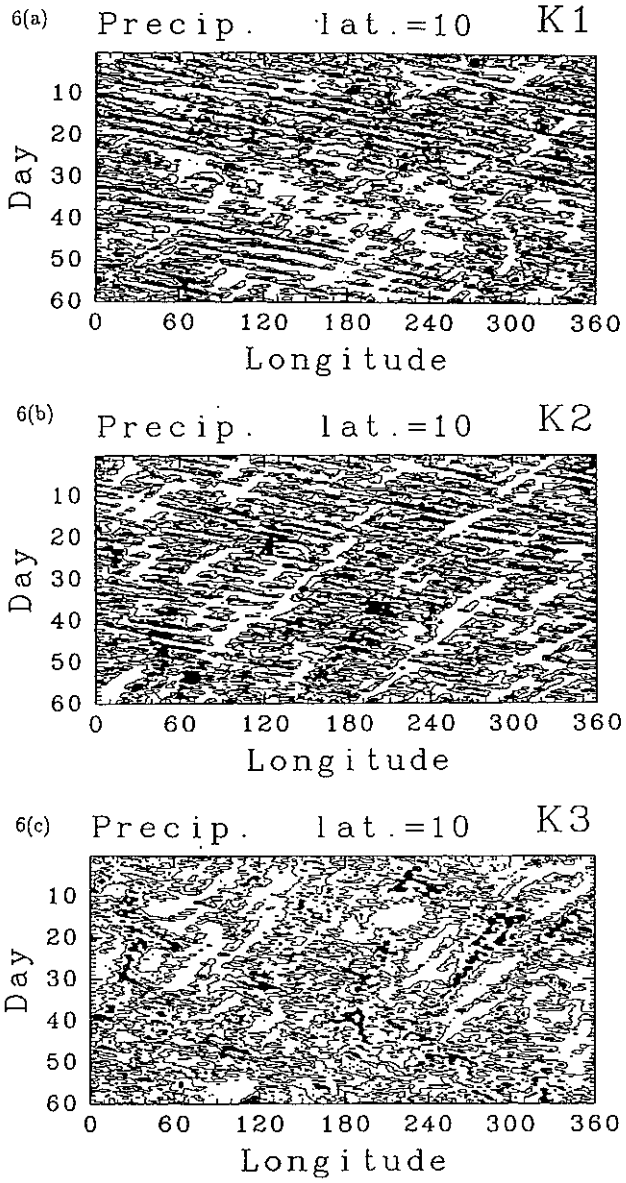

Fig. 6. Longitude–time distributions of precipitation at 10 degrees north. Contours indicate 2 mm/day and areas of over 10 mm/day are shaded. (a) Standard experiment K1, (b) high SST experiment K2, (c) low SST experiment K3.

eastward-moving precipitating areas are identified more clearly, moving around the circle in about 20 days. The planetary scale structure is hardly seen, as in the case of the equator (see Part I). Instead, the precipitation intensity is modulated by another system which moved westward. There are remarkable areas of suppressed precipitation which have a scale of around 1000 km and move westward at a speed of about 5 m/s. Such areas are also recognizable in experiment K1. In the low SST experiment K3 (Fig. 6c), the eastward-moving precipitating areas are traceable but not clear. The planetary scale structure exists and corresponds to that at the equator (Fig. 3c in Part I, also refer to Fig. 3a).

In the ITCZ region of the real atmosphere, westward-moving signals with the easterly wave disturbance is dominant in OLR data (Nakazawa, 1986). The behavior of precipitation in experiments K1 and K2 is considerably different from that in the real atmosphere. HS86 overlooked such an unrealistic behavior of the model.

3.3 Structure of circulation associated with the eastward-moving grid scale precipitating areas at 10 degrees latitude

The structure of the circulation associated with the eastward-moving grid scale precipitating areas at 10 degrees latitude is examined by composite technique. The composite is performed with reference to each longitude of peak[3] precipitation in order to pick up the structure associated with individual precipitating areas. The detailed method is described in Part I. In the following, the results of experiment K2 are mainly described, because the eastward movement of grid scale precipitating areas is the clearest in this experiment among three experiments.

Figure 7a shows the composite structure of the precipitation itself. The longitudinal scale is about 1000 km and the meridional scale is even smaller. The precipitation at the same longitude in the ITCZ of the other hemisphere is slightly suppressed. The composite structure of the longitude-height section (Figs. 7b–7d) looks generally similar to that associated with the precipitating area at the equator (Figs. 8 in part I). The common characteristics are the existence of a warm region from upper levels near the precipitation peak to lower levels to the east of the peak, the existence of a cold region from lower levels near the precipitation peak to upper levels to the west of the peak, and the slantwise structure of upward motion. However, the westward slant of the phase is comparatively weak. There is a region of large positive vorticity in the lower levels a little west to the precipitation peak (Fig. 7d). The updraft to the east of the vorticity center is considered to responsible for generating vorticity by stretching effect. Note that the magnitude of vorticity at upper levels is very weak. The horizontal structure at the lower levels (Fig. 8a) shows a character of an eastward-propagating inertio-gravity wave, that is, the correspondence of westerly wind and high pressure. The structure at upper levels (Fig. 8b) is remarkably different from that at lower levels. The outflow is significantly isotropic at upper levels.

In order to clarify the behavior of vorticity sig-

[3]This peak does not necessarily mean the peak in the longitudinal-latitudinal plane or in the longitude-time section. It only means that the precipitation at that gridpoint is largest among several gridpoints of different longitude nearby at the same latitude and time.

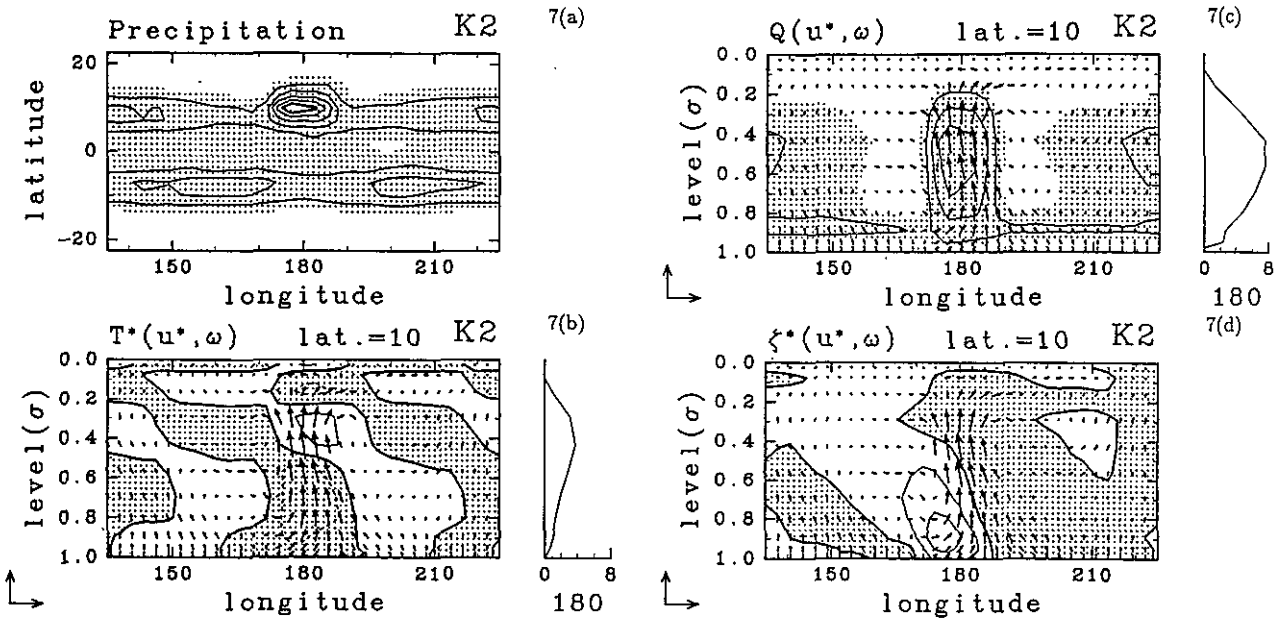

Fig. 7. Composite structure with reference to precipitation peaks at 10 degrees north of experiment K2. (a) Horizontal distribution of precipitation. The contour interval is 4 mm/day and areas of over 2 mm/day are shaded. (b) Longitude–height section of temperature (contour) and wind vectors at 10 degrees north. Zonal means are subtracted for temperature and zonal wind. The contour interval is 0.2K and negative areas are shaded. (c) Longitude–height section of heating by cumulus (contour) and wind vectors at 10 degrees north. Zonal mean is subtracted for zonal wind. Contour interval is 2K/day and areas of over 1K/day are shaded. Plot on the right side is the vertical distribution of heating (Unit; K/day) at the precipitation peak. (d) Longitude–height section of relative vorticity (contour) and wind vectors at 10 degrees north. Zonal means are subtracted for vorticity and zonal wind. The contour interval is $2\times10^{-6}s^{-1}$ and negative areas are shaded. In each figure, the unit vectors shown at the left side bottom represent 5 m/s and 5 mb/hr respectively.

nals associated with the precipitation, the longitude-time distribution of vorticity is plotted in Fig. 9. At lower level $\sigma=0.95$, the westward-moving structures of grid scale are significant. The areas of suppressed precipitation appearing in Fig. 6b apparently correspond to the regions of negative vorticity. On the other hand, the precipitation is enhanced in the regions of positive vorticity (for example, around 180 degrees of day 40–50). The eastward movement of grid scale areas of positive vorticity can be recognized, although rather intermittently. Those areas correspond to the positive vorticity appearing in the composite (Fig. 7d). There seems to be no regular structure in the vorticity field in the upper layer (not shown). To pick up the structure associated with the westward-moving low level vorticity signal, a composite is made using the longitude of peak vorticity as a key. The result is Fig. 10, which clearly shows the concentration of vorticity at lower levels.

The easterly wave disturbances in the real atmosphere are westward-moving disturbances associated with large vorticity and cumulus activity. There indeed exist westward moving disturbances of vorticity in the model, yet the vorticity is concentrated in the lower troposphere and only associated with the modulation of precipitation. This behavior is quite different from that of the real atmosphere where the direct coupling between westward-moving disturbances and precipitation occurs, although some evidence for the modulation of precipitation by an eastward-propagating mode is observed (Nakazawa, 1986; Takayabu and Murakami, 1991).

The comparison of composite structures with reference to the precipitation peaks at 10 degrees latitude shows little difference between experiments K2 and K1 (not shown). For experiment K3, the composite structure is unclear, corresponding to the fact that the movement of grid scale precipitating areas is not regular in this experiment.

4. An experiment with moist convective adjustment

4.1 Eastward-propagating planetary scale structure around the equator

A distinct structure of wavenumber one appears in the composite fields with reference to a point which is moving at a constant speed of 8.5 m/s (Fig. 11). The main difference from the experiment with Kuo's parameterization (Fig. 2) is the reversal of the sign of temperature deviation at around $\sigma=0.9$ level. The

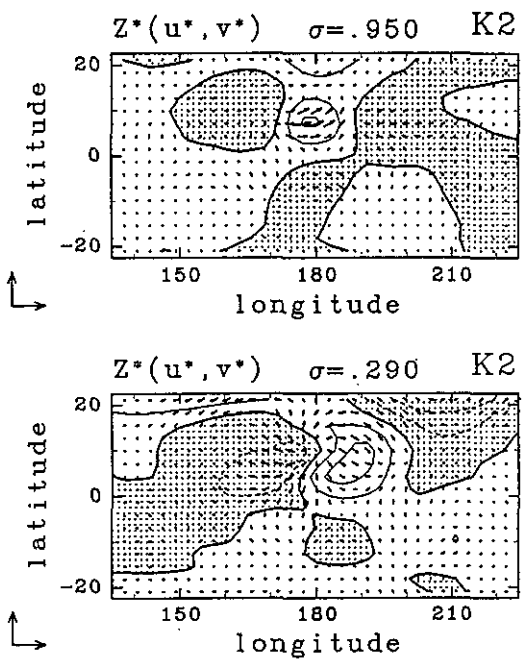

Fig. 8. Longitude–latitude sections of height field equivalent to the field of a constant p surface $Z(\sigma)+g^{-1}RT\ln p_s$ (contour) and wind vectors in composite with reference to precipitation peaks at 10 degrees north in experiment K2. Zonal means are subtracted for all quantities. The contour interval is 1 m and negative areas are shaded. The unit vectors shown at the left side bottom represent 5 m/s for both directions. (a) $\sigma=0.95$ (about 950 mb), (b) $\sigma=0.29$ (about 290 mb).

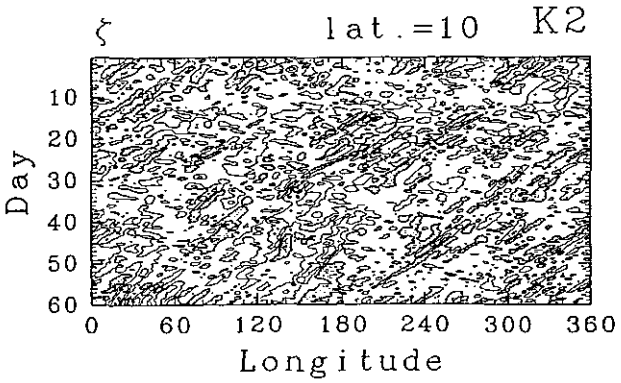

Fig. 9. Longitude–time section of relative vorticity at 10 degrees north and $\sigma=0.95$ in experiment K2. The contour interval is 1 $\times 10^{-5}\mathrm{s}^{-1}$ and negative areas are shaded.

reversal may be caused by the low level cooling due to moist convective adjustment. An interesting feature of Fig. 11b is that the region of intense heating becomes restricted to the lower levels as we move eastward from the center of precipitation.

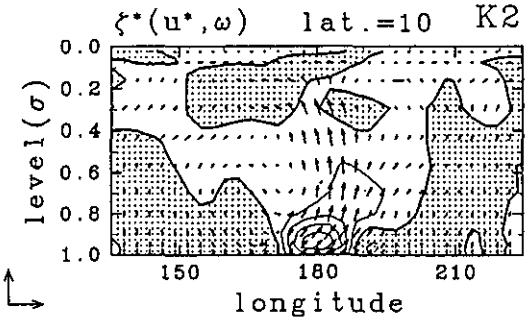

Fig. 10. Longitude–height section of relative vorticity (contour) and wind vectors at 10 degrees north in the composite with reference to peaks of positive vorticity at 10 degrees north in experiment K2. Zonal means are subtracted for vorticity and zonal wind. The contour interval is $2\times 10^{-6}\mathrm{s}^{-1}$ and negative areas are shaded.

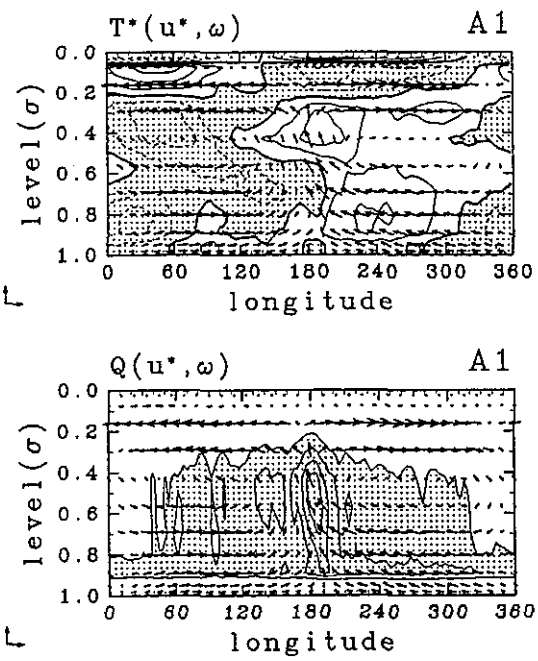

Fig. 11. Composite structure in experiment A1 with reference to a point moving at a constant speed (8.5 m/s). (a) Longitude–height section of temperature (contour) and wind vectors at the equator. Zonal means are subtracted for temperature and zonal wind. The contour interval is 0.2K and negative areas are shaded. (b) Longitude–height section of cumulus heating (contour) and wind vectors at the equator. Zonal mean is subtracted for zonal wind. The contour interval is 1K/day and areas of over 1K/day are shaded. In each figure, the unit vectors shown at the left side bottom represent 5 m/s and 2.5 mb/hr respectively.

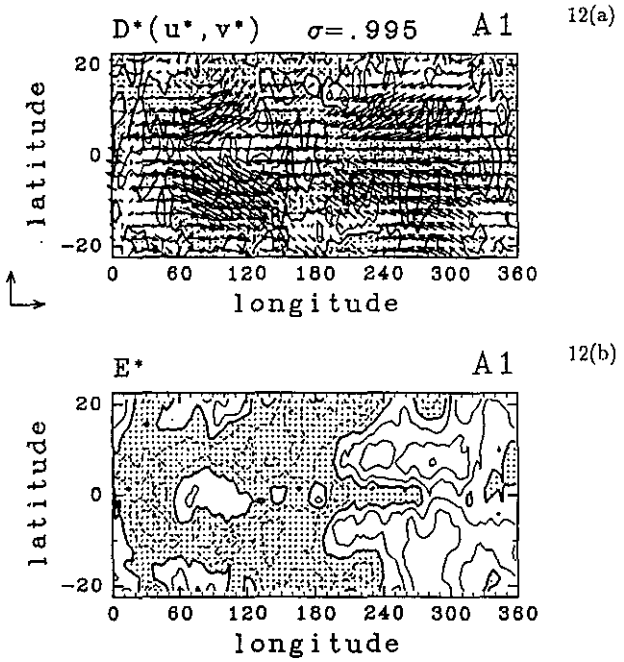

Fig. 12. Horizontal distributions of divergence and evaporation in experiment A1 in the composite with reference to a point moving at a constant speed (8.5 m/s). (a) Divergence (contour) and wind vectors at σ =0.995 (about 995 mb). Zonal means are subtracted for all quantities. The contour interval is $1\times10^{-6}s^{-1}$ and negative (convergence) areas are shaded. The unit vectors shown at the left side bottom represent 2.5 m/s for both directions. (b) Evaporation from surface. Zonal mean is subtracted. The contour interval is 5 W/m^2 (corresponds to about 0.2 mm/day precipitation) and negative areas are shaded.

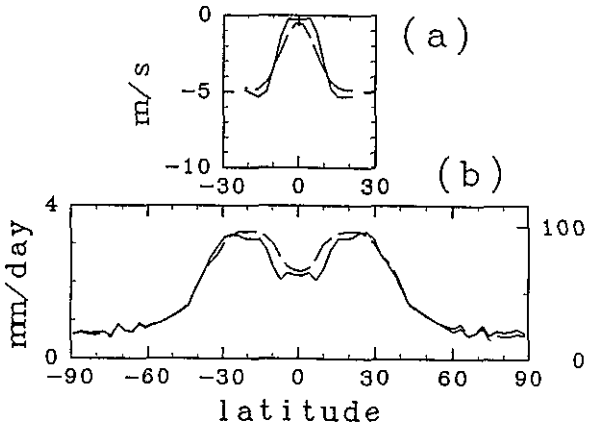

Fig. 13. Zonal and time mean distributions of surface zonal wind [u] and evaporation [E] fields. Solid line; standard experiment K1. Broken line; experiment with moist convective adjustment A1. (a) Zonal wind [u]. at σ=0.995 (about 995 mb). Unit is m/s. (b) Evaporation [E]. Unit is mm/day (left) and W/m^2 (right).

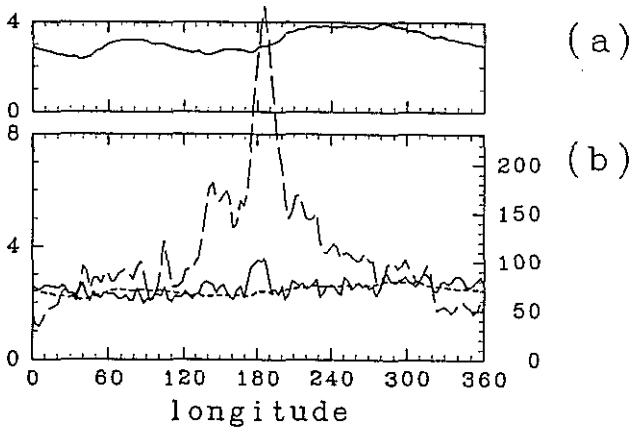

Fig. 14. Longitudinal distributions of variables related to the heating in experiment A1 averaged around the equator (+10°~ −10°) in the composite, with reference to a point moving at a constant speed (8.5 m/s). (a) Absolute value of wind speed near the surface (σ=0.995, about 995 mb). Unit is m/s. (b) Dotted line; evaporation. Broken line; precipitation (vertically integrated heating). Solid line; vertically integrated heating from which the adiabatic cooling is subtracted. Unit is mm/day (left) and W/m^2 (right).

Figure 12 represents the composite distribution of divergence at the lowest levels and evaporation. Distinct structures of wavenumber one are seen, with a positive anomaly to the east of the center (about 180 degrees) both in the fields of convergence and evaporation. The meridional convergence and divergence is apparent and has a large amplitude around the equator, which agrees with the characteristics of the model of Wang (1988). The magnitude of evaporation anomalies is largest at about 8 degrees latitudes. The longitudinal variation is about 20 % of the zonal mean value which is shown in Fig. 13b. Figure 14 represents the composite longitudinal distribution of the absolute value of surface wind speed, evaporation, and precipitation averaged between 10 degrees north and 10 degrees south. The precipitation is rather large to the east of the peak located around 180 degrees. The effective warming rate that is the difference between the heating rate by cumulus and the adiabatic cooling rate by upward motion is slightly larger to the east of the peak than to the west. The phase relationship among these quantities is similar to the results of experiment K3 (Fig. 5), and the energy is supplied to the disturbances by the net heating associated with cumulus convection.

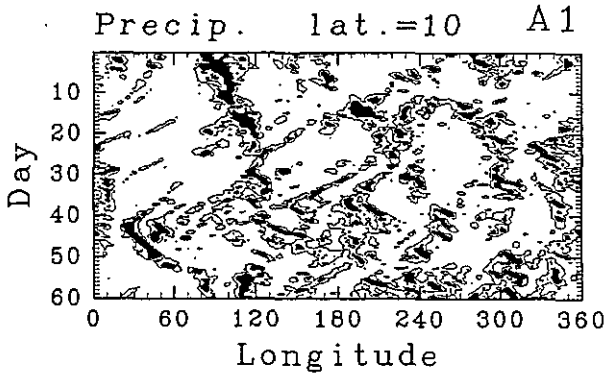

Fig. 15. Longitude–time distribution of precipitation at 10 degrees north in experiment A1. Contours indicate 2 mm/day and areas of over 10mm/day are shaded.

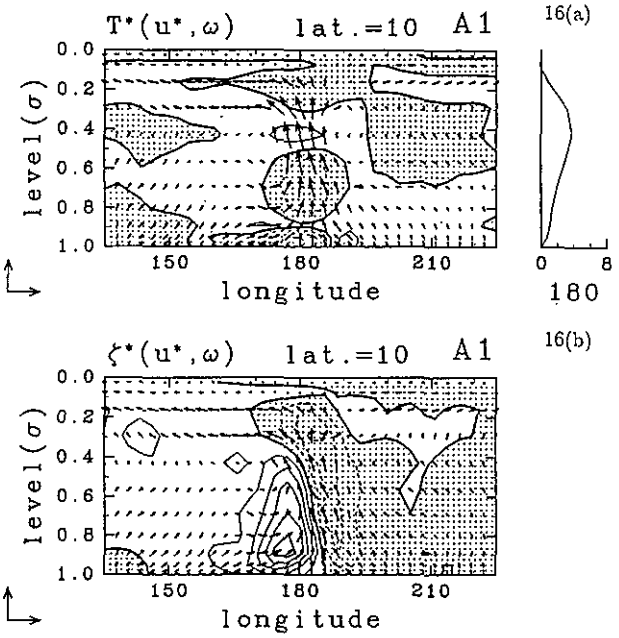

Fig. 16. Composite structure with reference to precipitation peaks at 10 degrees north in experiment A1. (a) Longitude–height section of temperature (contour) and wind vectors at 10 degrees north. Zonal means are subtracted for temperature and zonal wind. The contour interval is 0.2K and negative areas are shaded. (b) Longitude–height section of relative vorticity (contour) and wind vectors at 10 degrees north. Zonal means are subtracted for vorticity and zonal wind. The contour interval is 2 $\times 10^{-6}$s^{-1} and negative areas are shaded. In each figure, the unit vectors shown at the left side bottom represent 5 m/s and 5 mb/hr respectively.

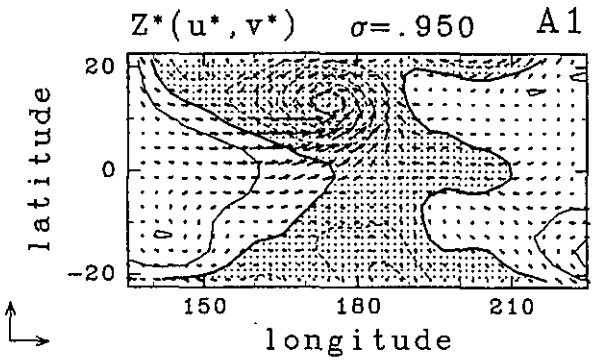

Fig. 17. Longitude–latitude section of height field equivalent to the field of a constant p surface $Z(\sigma) + g^{-1}R\mathcal{T}\ln p_s$ (contour) and wind vectors at σ=0.95 in the composite with reference to precipitation peaks at 10 degrees north in experiment A1. Zonal means are subtracted for all quantities. The contour interval is 1m and negative areas are shaded. The unit vectors shown at the left side bottom represent 5 m/s for both directions.

4.2 Longitude–time distribution of precipitation at 10 degrees latitude

At the equator, there are large differences between experiment A1 and experiments K1$\sim$K3 in the behavior of grid scale precipitating areas, as stated in part I. The behavior of grid scale precipitating areas at 10 degrees latitude in experiment A1 (Fig. 15) is also different from that in experiments K1$\sim$K3. There exist eastward-moving areas, but their lifetime is much shorter than that in experiment K1 or K2. Note that there are westward moving precipitating areas with a rather long life time, for example around 180 degrees longitude at day 30.

4.3 Structure of circulation associated with the grid scale precipitation areas at 10 degrees latitude

The composite structure associated with the grid scale precipitation areas at 10 degrees latitude in experiment A1, which is produced by the same method in the case of K2 (Fig. 7), is shown in Fig. 16. This structure looks very different from that in experiment K2. The westward slant of the phase line is hardly recognizable and strong vorticity signals exist even in the upper troposphere. There is large positive vorticity to the west of the updraft which is largest in the lower layer and extends upward to the middle layer, and negative vorticity rather east of the updraft in the upper layer. The horizontal structure (Fig. 17) clearly shows the existence of vortices.

These characteristic features at 10 degrees latitude in experiment A1 are rather similar to the features of easterly wave disturbances (Reed and Recker, 1971). The westward movement of vorticity is apparent in the longitude–time plot of vortic-

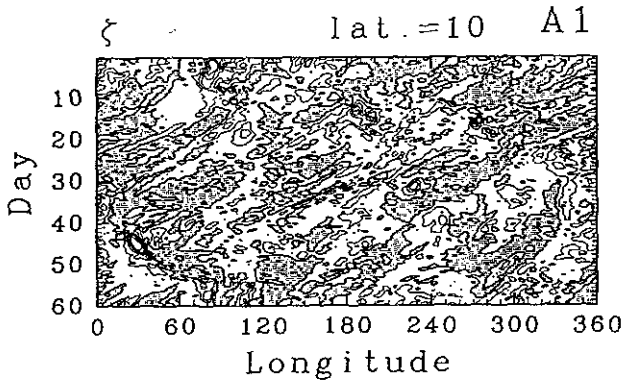

Fig. 18. Longitude–time distribution of relative vorticity at 10 degrees north and $\sigma = 0.95$ in experiment A1. The contour interval is $1 \times 10^{-5} s^{-1}$ and negative areas are shaded.

ity (Fig. 18), and vortices coupled with precipitation can be found by comparing it with the longitude–time plot of precipitation (Fig. 15).

5. Discussion

5.1 Eastward-propagating planetary scale structure around the equator

In experiments K1∼K3, the planetary scale structure around the equator is shown to exist as a modulation of the grid scale precipitating areas ('super clusters'). In each experiment, there is little difference in the speed of movement between the grid scale precipitating areas and the planetary scale structure as described in Part I of this paper (see Fig. 3 of Part I). From these results, one may consider that the propagation of the planetary scale structure is realized by the movement of the group of grid scale precipitating areas, and may agree with HS86's interpretation. However, the results shown in Part I indicate the dependences of the activity of the two structures on the SST value are opposite: The activity of super clusters becomes unclear when the SST is decreased, while the activity of the planetary scale structure becomes obscure when the SST is increased. Thus, we have to consider a maintenance mechanism peculiar to the planetary scale structure.

In the experiment with moist convective adjustment A1, a planetary scale structure exists clearly and shows distinct eastward propagation without the co-existence of an eastward-moving grid scale structure. This result may give some hints about the dynamics of the eastward-propagating planetary scale structures. If the planetary scale eastward-moving structure in experiment A1 is considered to be the counterpart of the planetary scale structure in experiments K1∼K3, it can be concluded that the existence of the eastward-moving grid scale precipitating areas is not indispensable for the existence

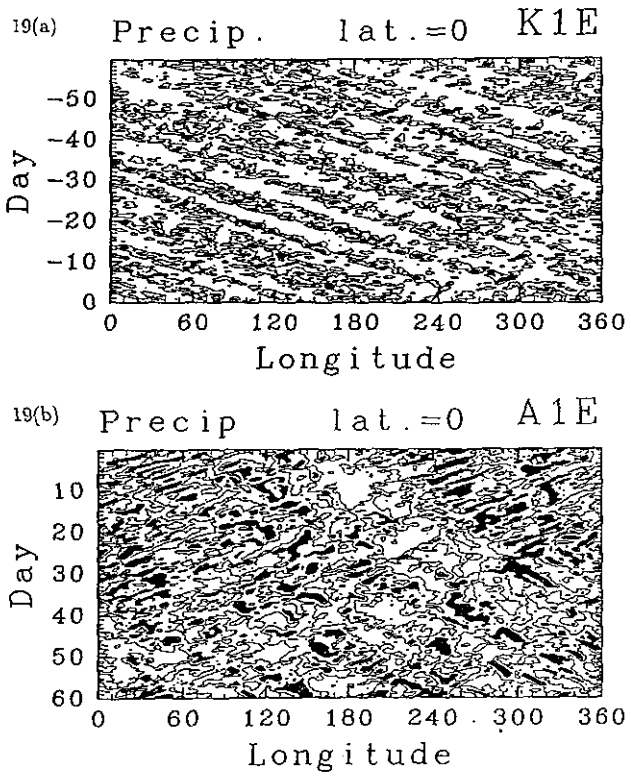

Fig. 19. Longitude–time distributions of precipitation at the equator in the experiments with zonally averaged bulk transfer coefficient ($[C_D|v|]$). Contours indicate 2 mm/day and areas of over 10 mm/day are shaded. (a) Experiment K1E which corresponds to K1, (b) experiment A1E which corresponds to A1.

of the planetary scale structure.

There is a distinct region of large convergence in the planetary boundary layer to the east of planetary scale precipitating regions in experiment A1 (Fig. 12a). This supports the frictional CISK interpretation by Wang (1988). The evaporation is also larger to the east of the precipitating region corresponding to the strong surface easterly (Fig. 12b). This agrees with the evaporation–wind feedback theory by Emanuel (1987) and Neelin *et al.* (1987). In experiment K3, there is also a region of large convergence and evaporation to the east of active regions of precipitation (Fig. 3). This suggests that the eastward-moving planetary scale structure in K3 or K1 corresponds to the large scale structure in A1 with respect to the mechanism of maintenance, which is not directly related to the maintenance of the grid scale structure.

Additional experiments are performed in order to clarify this point. The evaporation–wind feedback can be removed by using the zonal mean value of bulk transfer coefficient $C_D|v|$ instead of the local value in the expression for evaporation Eq. (1).

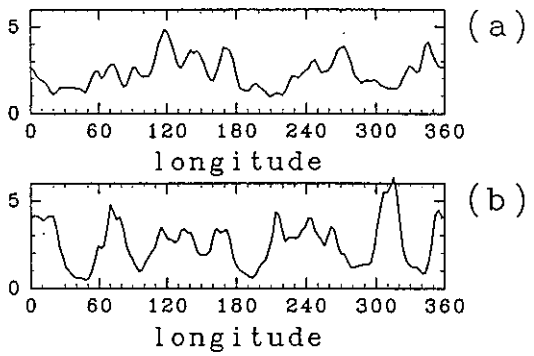

Fig. 20. Longitudinal distributions of precipitation at the equator in the composite with reference to a point moving at constant speed (12 m/s). (a) Standard experiment K1, (b) experiment K1E with zonally averaged bulk transfer coefficient ($[C_D|v|]$).

This is virtually the same method that Neelin *et al.* (1987) adopted. In the same way as K1∼A1, the model is integrated for 120 days and the data of the last 60 day period is used for analyses. Figure 19b shows the result of the experiment using the moist convective adjustment scheme (A1E) which is the same condition as experiment A1 (Fig. 1b) except for the above modification. The disappearance of planetary scale structure is apparent. Figure 19a is the result of experiment K1E which is identical to experiment K1 (Fig. 1a) but with the feedback removed. In order to clarify the difference, longitudinal distributions of composite precipitation around the equator in experiments K1 and K1E are plotted in Fig. 20. In experiment K1 (Fig. 20a), a planetary scale structure which has a maximum of precipitation around 120 degrees longitude and a minimum at about 300 degrees longitude can be clearly seen, even though small scale structure is superimposed. In experiment K1E (Fig. 20b), on the other hand, the amplitude of planetary scale structure is significantly decreased whereas the eastward-moving grid scale precipitating areas are still clearly, or even more clearly observed. Thus we see that the existence or non-existence of evaporation–wind feedback does not alter qualitatively the behavior of grid scale precipitating areas. This statement also holds concerning the precipitation at 10 degrees latitude (not shown). It is concluded that there exist maintenance mechanisms peculiar to planetary scale structures and the evaporation–wind feedback is an essential part of the mechanism, at least in the model. Unfortunately, the effect of frictional convergence has not been successfully separated and the importance of it has not been identified.

These results including the discussions of Part I suggest that the hierarchical structure composed of the grid scale precipitating areas and the planetary scale modulation in the model is maintained by the coexistence of at least two different maintenance mechanisms of disturbances, *i.e.*, wave-CISK and evaporation–wind feedback. It is found in Part I that the speeds of eastward movement of the both structures are approximately the same but the dependences of the strength of the two structures on the SST value is opposite. It can be considered that there exists a certain kind of interaction between the two structures. However, the results of experiment A1 suggest that this interaction is not strong: The existence of the one feature does not rely on the existence of the other, which is contrary to the statement of HS86.

The result that the evaporation-wind feedback mechanism dominates in the planetary scale while other mechanisms such as wave-CISK dominate in the comparatively small scale is very informative. According to the linear theory of wave-CISK, a preference for small scale structures is naturally expected. It can be imagined that the relative importance of the evaporation in the moisture budget increases as the scale of the region increases: The evaporation term will be proportional to the square measure of the region, whereas the convergence term due to circulation will be proportional to the circumference of the region. Hence, we may speculate that the relative importance of evaporation–wind feedback process to the wave-CISK process increases as the scale increases. Nevertheless, however, the selection of the planetary scale, especially the wavenumber one, by the evaporation–wind feedback mechanism cannot be explained by ordinary linear theories (Emanuel, 1987; Neelin *et al.*, 1987). Yano and Emanuel (1991) presented a model in which the growth of small scale disturbances is suppressed owing to the large energy outflow by wave propagation into the stratosphere. It has not been explored in our model whether such a mechanism is effective for the scale selection. A model with sufficient resolution in the stratosphere must be utilized in order to verify the applicability of their model.

5.2 Nature of precipitation at the ITCZ

In experiments K1∼K3, the existence of a double ITCZ structure is remarkable. At the latitude of peak precipitation (10 degrees), precipitation occurs in the form of eastward-moving precipitating areas. The circulation structure associated with the precipitating areas at this latitude resembles the structure of eastward-propagating inertio-gravity wave. Furthermore, the phase relationship between heating and circulation is similar to that associated with the grid scale precipitating areas at the equator. It is considered that this circulation associated with precipitating areas is maintained by the wave-CISK mechanism.

The disturbance which is commonly observed at

the ITCZ latitudes in the real atmosphere is the easterly wave disturbance, which moves westward with cumulus activity. The main difference in structure between easterly wave disturbances and the eastward-moving disturbances in the model is the distribution of the vorticity. There are deep vorticity signals associated with the actual easterly wave disturbances (Reed and Recker, 1971), whereas the amplitude of vorticity is confined to the low levels in the eastward-moving disturbances in experiments K1~K3. This difference in the depth of the vorticity distribution may be attributed to the difference in the mean vorticity field. In the actual atmosphere, there is nonzero absolute vorticity in the mean field so that the vortex can be created by a heat source through stretching and shrinking. But the absolute vorticity in the upper layer of the model tropics is nearly zero (refer to part I) and a vortex cannot be created easily there.

At 10 degrees latitude in experiments K1~K3, vorticity signals exist in the lower levels for a long time and move westward, driven by an easterly wind. However, the precipitation is not directly coupled with these vorticity signals in experiments K1 ~K3. It is coupled with the eastward-propagating inertio-gravity waves. The vorticity causes only the amplification and suppression of precipitation as an amplitude modulation. Unfortunately, it is still unclear whether or not this amplification and suppression of precipitation is responsible for the maintenance of the double ITCZ structure as hypothesized by Charney (1969).

It has been already confirmed that the evaporation–wind feedback mechanism is very important in the maintenance of a certain kind of large scale precipitating structure. Inspection of the zonal mean field in this respect suggests another mechanism of the maintenance of the double ITCZ structure. The amount of evaporation at the equator is somewhat smaller than that at 10 to 15 degrees latitude, as seen in Fig. 4b. It is possible that this latitudinal contrast of evaporation is responsible for the existence of the double ITCZs. The minimum of evaporation at the equator is considered to be caused by a weakness of the surface wind there (*see* Fig. 4a). This suggests the existence of a process which can be called 'evaporation–wind feedback for the zonal mean field'. The possible feedback for the zonal mean field can be removed by averaging the bulk transfer coefficient $C_D|v|$ not only longitudinally but also latitudinally, in the same way as we did for removing the feedback for the planetary scale disturbances. Figure 21 represents the results of experiment K1T, which is identical to experiment K1 except that a longitudinally and latitudinally averaged bulk transfer coefficient is used between 30 degrees north and 30 degrees south. The resulting precipitation is concentrated at the equator and the

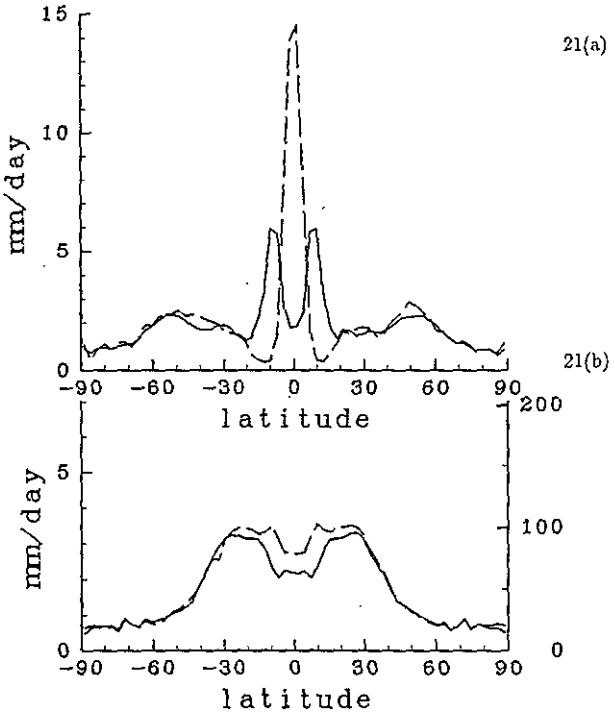

Fig. 21. Latitudinal distributions of time and zonal mean precipitation and evaporation. Solid line: standard experiment K1. Broken line: experiment K1T with latitudinally averaged bulk transfer coefficient ($[\overline{C_D|v|}]^{\varphi}$). (a) Precipitation, (b) evaporation. Unit is mm/day (left) and W/m^2 (right).

double ITCZ structure has disappeared. The latitudinal contrast of evaporation becomes rather weak. From these results, it is strongly suggested that the dependence of evaporation on wind speed is an important factor for the maintenance of the zonal mean field.

A single ITCZ structure appeared in the experiment by Lau *et al.* (1988). The SST distribution they used is the time and zonal mean field of the result of a swamp experiment (experiment with zero surface heat capacity), which is quite different from ours. Another experiment with an SST distribution which is obtained in the same manner as Lau *et al.* (1988) is performed with our model by using Kuo's parameterization. In this experiment, the single precipitation belt at the equator has appeared (not shown). The difference in SST between the equator and 10 degrees latitude is about 2K in this experiment, while the difference is only 0.5K in our standard SST distribution. In the case of swamp experiments or the experiments using the SST distributions derived from swamp experiments, the amount of latent energy supply from the ocean surface into the atmosphere is approximately the same as the net radiation at the surface and has a maximum at the equator in the equinox condition. This means

that, in the swamp experiment, the SST should be significantly higher at the equator than at the non-equatorial latitudes when the wind speed is smaller at the equator. If the difference in SST between 10 degrees latitude and the equator is not as large as the case of swamp condition, the latent energy supply at the equator cloud be smaller than those at 10 degrees latitude. Thus the amount of precipitation at 10 degrees latitude is expected to be larger than that at the equator only when the difference in SST is sufficiently small. The tendency of the precipitation at off-equatorial latitudes to be larger when the SST contrast is sufficiently small is prominent in the experiments with Kuo's parameterization. When we use the moist convective adjustment, this tendency becomes weaker. The result of the experiment by Manabe *et al.* (1974) which shows that the ITCZ follows the maximum latitude of SST does not contradict our results, because the parameterization they used is the moist convective adjustment scheme.

Recently, Sumi (1991) investigated the behavior of precipitating areas in GCM with globally uniform SST distribution. It is shown that a double ITCZ structure centered at the equator appears even if the meridional gradient of SST is zero. He claimed that the frictional CISK mechanism associated with vortices is the most important factor in determining the location of ITCZs in such a situation. In our experiments, the characteristics of the general circulation are greatly different from that of Sumi's (1991) experiments in many respects because of the difference of meridional SST gradient. What we emphasize here is that, in order to describe the circulation characteristics of our experiments, the meridional inhomogeneity of the moisture budget must be considered in addition to latitudinal dependence of dynamical properties. Further investigations concerning this problem will be presented in subsequent papers.

The results of the experiments with Kuo's parameterization show unrealistic dominance of eastward-moving precipitating areas at the ITCZs. Because of this, one may consider that Kuo's parameterization tends to exaggerate the nature of producing the wave-CISK mechanism compared with other schemes or the real atmosphere. However, it is dangerous to connect this result directly to the judgement of the superiority of a particular cumulus parameterization because the results probably change when parameterizations of other physical processes and the resolution of the model are changed.

6. Conclusions

The characteristics of cumulus activity and their parameter dependence in the 'aqua planet' GCM experiments are examined, concentrating on the planetary scale structure and the structure of the precipitating areas around the ITCZ regions.

The eastward-moving structures on the planetary scale can be similarly recognized in the experiments with two different cumulus parameterization schemes, *i.e.*, Kuo's scheme and the moist convective adjustment. The structures of circulation on the planetary scale in the two experiments look basically similar, although the behavior of precipitation on the synoptic scale is remarkably different. Further, the results of the experiments with Kuo's parameterization show a tendency that the planetary scale structure is more prominent when the activity of the grid scale precipitating areas is low. These results do not support HS86's explanation of the existence of the planetary scale structure by the feedback of the non-uniformity in the distribution of the grid scale precipitating areas. The results of the analyses of the circulation structure suggest that the frictional CISK and/or the evaporation–wind feedback mechanism is effective for the maintenance of the eastward-propagating planetary scale structure.

When the evaporation–wind feedback process is artificially removed, the eastward-moving planetary scale modulation structure almost disappears. Thus the planetary scale structure is considered to be maintained by the evaporation–wind feedback mechanism to a certain extent. The fact that the grid scale structures still exist without evaporation–wind feedback process in the experiment using Kuo's scheme suggests that the evaporation–wind feedback is comparatively ineffective and other processes such as wave-CISK are more important for structures of small time and spatial scales in the model. It is concluded that the hierarchical structure composed of the grid scale precipitating areas (super clusters) and the planetary scale modulation (30 day oscillation) in the model is maintained by the coexistence of at least two maintenance mechanism of different nature, *i.e.*, wave-CISK and evaporation–wind feedback. Unfortunately, the role of the frictional CISK mechanism has not been clarified because we could not treat that process separately.

In the experiments with Kuo's parameterization, the precipitation at the double ITCZs occurs in the form of eastward-moving precipitating areas. They are considered to be maintained by the wave-CISK mechanism, although the inertio-gravity wave mode is dominant instead of the Kelvin wave at the equator. This feature is quite different from the easterly wave disturbances in the real atmosphere. Because of this discrepancy, Kuo's parameterization in the model may be considered to enhance artificially the wave-CISK mechanism. In the experiment with moist convective adjustment, the ITCZ is not clearly separated into two bands and eastward-moving precipitating areas are not evident at 10 degrees latitude. Instead, there are westward-moving vortices which are coupled with precipitation and resemble well the easterly wave disturbances observed in the

real atmosphere.

As for the mechanism of the separation of the ITCZ into double bands, the explanation concerning the latitudinal difference of efficiency of frictional CISK was presented by Charney (1969). Amplification and suppression of precipitation associated with westward-moving vortices can be recognized in the results of the experiment with Kuo's parameterization. However, this does not necessarily support Charney's idea because the precipitating areas are dominated by the structure of the wave-CISK mode. On the other hand, it is revealed that the dependence of evaporation on wind speed has a large influence on the zonal mean structures. At the equator, the evaporation rate is small compared to the higher latitudes of the tropics because of the weakness of the surface wind there. It is demonstrated that the precipitation is concentrated at the equator and a single ITCZ forms when this dependence is artificially removed.

In summary, in our model experiments, it is clarified that the disturbances on synoptic or small scale in the model are tightly associated with precipitation, and direct coupling processes between the circulation and cumulus heating, such as wave-CISK mechanism, play an important role in their formation and maintenance. It is also suggested that the budget of moisture, which is strongly affected by evaporation rate, is the primarily important factor for the formation and maintenance of planetary scale structures. Unfortunately, these results depend rather strongly on the parameterization schemes utilized in the model. As for the disturbances on the synoptic or small scale, different cumulus parameterization promotes different types of disturbances. The characteristics of the planetary scale structures is expected to depend not only on cumulus parameterization but also on parameterizations of the surface fluxes, the vertical diffusion and the radiative processes. For further understanding of tropical circulation fields, observational estimates of the moisture and energy budgets on various time and spatial scales are required. Moreover, extensive examinations on the dependence of model results on the parameterizations of physical processes and external parameters are also desired.

Acknowledgements

The authors would like to thank Profs. T. Matsuno and A. Sumi for valuable discussions and encouragement, and Mr. N. Sato of the Japan Meteorological Agency for providing the original model code. Comments by Prof. K. Emanuel and anonymous reviewers are helpful to improve the original manuscript. Discussions with Dr. S.-P. Xie and Mr. K. Nakajima were also helpful. This research was supported by a Grant-in-Aid, Ministry of Education, Science and Culture. The computation was made on HITAC-S820 and M-680H computers of the Computer Center, University of Tokyo. For drawing the figures, the GFD-DENNOU Library produced by Drs. M. Shiotani and S. Sakai was used.

References

Chang, C.-P. and H. Lim, 1988: Kelvin wave-CISK: A possible mechanism for the 30–50 day oscillations. *J. Atmos. Sci.*, **45**, 1709–1720.

Charney, J.G. and A. Eliassen, 1964: On the growth of the hurricane depression. *J. Atmos. Sci.*, **21**, 68–75.

Charney, J.G., 1969: The intertropical convergence zone and the Hadley circulation of the atmosphere. *Proceedings of WMO/IUGG Symposium on Numerical Wether Prediction in Tokyo.*, III-73–III-79, Japan Meteorological Agency.

Emanuel, K.A., 1987: An air-sea interaction model of intraseasonal oscillations in the tropics. *J. Atmos. Sci.*, **44**, 2324–2340.

Hayashi, Y. 1970: A theory of large-scale equatorial waves generated by condensation heat and accelerating the zonal wind. *J. Meteor. Soc. Japan*, **48**, 140–160.

Hayashi, Y.-Y. and A. Sumi, 1986: The 30–40 day oscillations simulated in an "aqua planet" model. *J. Meteor. Soc. Japan*, **64**, 451–467.

Hubert, L.F., A.F. Krueger and J.S. Winston, 1969: The double intertropical convergence zone—fact or fiction? *J. Atmos. Sci.*, **26**, 771–773.

Itoh, H., 1989: The mechanism for the scale selection of tropical intraseasonal oscillations. Part I: Selection of wavenumber 1 and the three-scale structure. *J. Atmos. Sci.*, **46**, 1779–1798.

Kanamitsu, M., K. Tada , T. Kudo, N. Sato and S. Isa, 1983: Description of the JMA operational spectral model. *J. Meteor. Soc. Japan*, **61**, 812–827.

Knutson T.R., K.M. Weickmann, 1987: 30–60 day atmospheric oscillations: Composite life cycles of convection and circulation anomalies. *Mon. Wea. Rev.*, **115**, 1407–1436.

Kuo, H.L., 1974: Further studies of the parameterization of the influence of cumulus convection on large-scale flow. *J. Atmos. Sci.*, **34**, 1232–1240.

Lau, K.-M. and L. Peng, 1987: Origin of low-frequency (intraseasonal) oscillations in the tropical atmosphere. Part I: Basic theory. *J. Atmos. Sci.*, **44**, 950–972.

Lau, N.-C., I.M. Held and J.D. Neelin, 1988: The Madden-Julian oscillation in an idealized general circulation model. *J. Atmos. Sci.*, **45**, 3810–3832.

Madden, R.A. and P.R. Julian, 1972: Description of global-scale circulation cells in the tropics with 40–50 day period. *J. Atmos. Sci.*, **29**, 1109–1123.

Manabe, S., D.G. Hahn and J.L. Holloway Jr., 1974: The seasonal variation of the tropical circulation as simulated by a global model of the atmosphere. *J. Atmos. Sci.*, **31**, 43–83.

Manabe, S., J. Smagorinsky and R.F. Strickler, 1965: Simulated climatology of a general circulation model with a hydrologic cycle. *Mon. Wea. Rev.*, **93**, 769–798.

Nakazawa T., 1986: Mean features of 30–60 day variations as inferred from 8-year OLR data. *J. Meteor. Soc. Japan*, **64**, 777–786.

Nakazawa, T., 1988: Tropical super clusters within intraseasonal variations over the western Pacific. *J. Meteor. Soc. Japan*, **66**, 823–839.

Neelin, J.D., I.M. Held and K.H. Cook, 1987: Evaporation-wind feedback and low-frequency variability in the tropical atmosphere. *J. Atmos. Sci.*, **44**, 2341–2348.

Numaguti, A. and Y.-Y. Hayashi, 1991: Behaviors of cumulus activity and the structures of circulations in an "aqua planet" model. Part I: The structure of the super clusters. *J. Meteor. Soc. Japan*, **69**, 541–561.

Pike, A.C., 1971: Intertropical convergence zone studied with an interacting atmosphere and ocean model. *Mon. Wea. Rev.*, **99**, 469–477.

Reed, R.J. and E.E. Recker, 1971: Structure and properties of synoptic-scale wave disturbances in the equatorial western Pacific. *J. Atmos. Sci.*, **28**, 1117–1133.

Rui, H. and B. Wang, 1990: Development characteristics and dynamic structure of tropical intraseasonal convection anomalies. *J. Atmos. Sci.*, **47**, 357–379.

Sumi A., 1991: Pattern formation of convective activity over the aqua-planet with globally uniform sea surface temperature (SST). Part I: Relationship between organization of convective activities and evaporation rate. (submitted to) *J. Meteor. Soc. Japan.*

Takayabu, Y.N. and M. Murakami, 1991: The structure of super cloud clusters observed in 1–20 June 1986 and their relationship to easterly waves. *J. Meteor. Soc. Japan*, **69**, 105–125.

Tokioka, T., K. Yamazaki, A. Kitoh and T. Ose, 1988: The equatorial 30–60 day oscillation and the Arakawa-Schubert penetrative cumulus parameterization. *J. Meteor. Soc. Japan*, **66**, 883–901.

Wang, B., 1988: Dynamics of tropical low-frequency waves: An analysis of the moist Kelvin wave. *J. Atmos. Sci.*, **45**, 2051–2065.

Wang, B. and J. Chen, 1989: On the zonal-scale selection and vertical structure of equatorial intraseasonal waves. *Quart. J. Roy. Meteor. Soc.*, **115**, 1301–1323.

Webster, P.J., 1983: Mechanisms of monsoon low-frequency variability: surface hydrological effects. *J. Atmos. Sci.*, **40**, 2110–2124.

Yano, J.-I. and K.A. Emanuel, 1991: An improved model of the equatorial troposphere and its coupling with the stratosphere. *J. Atmos. Sci.*, **48**, 377–389.

「水惑星」モデルにおける熱帯域の積雲活動のふるまいと循環構造
第2部　惑星規模の東進構造と熱帯収束帯

沼口　敦・林　祥介
（東京大学理学部地球惑星物理学教室）

「水惑星モデル」実験の結果を惑星規模の東進構造およびITCZ域における降水域の構造を中心に解析した。

30日振動、すなわち惑星スケールの東進構造は積雲パラメタリゼーションの種類にかかわらず現れる。その維持には海面蒸発の風速依存性すなわち蒸発－風速フィードバックが働いている可能性が高い。一方で、総観規模程度のスケールの構造には蒸発－風速フィードバックは効果的に働かず、wave-CISKのような他のメカニズムが重要となる。モデルにおける積雲活動の階層構造の存在にとって、2つの異なった擾乱維持メカニズムの共存が重要であることが示唆される。

Kuoのパラメタリゼーションを用いた実験で経度10度付近に存在する2本のITCZには、東進する1000 kmスケールの積雲活動域が持続的に存在する。これに対して湿潤対流調節を用いた実験では2本のITCZは不明瞭であるが、現実の大気での偏東風波動のような、渦度の西進にともなう積雲活動の西進が見られる。Kuoのパラメタリゼーションを用いた実験で顕著に見られたITCZの2本への分化には、平均場に対する蒸発－風速フィードバックと言うべきプロセスが介在していることが示される。